Clouds, Radiation, and the Diurnal Cycle of Sea Surface Temperature in the Tropical Western Pacific

PETER J. WEBSTER, CAROL ANNE CLAYSON, AND JUDITH A. CURRY

Program in Atmospheric and Oceanic Sciences, University of Colorado, Boulder, Colorado

(Manuscript received 17 March 1995, in final form 7 March 1996)

ABSTRACT

The relationship among clouds, surface radiation flux, and the sea surface temperature (SST) of the tropical western Pacific Ocean over the diurnal cycle is addressed in the context of the Atmospheric Radiation Measurement (ARM) Program scientific objectives for the tropical western Pacific Ocean. An understanding of the relationship between clouds and SST on a variety of time and space scales is needed to understand fully the cloud–radiation feedback in the tropical oceans and the maintenance of the warm pool. Here the diurnal cycle is emphasized. Data from the TOGA COARE Intensive Observation Period is examined and interpreted using an ocean mixed layer model that includes a parameterization of the "skin" temperature, explicit salinity, a surface heat budget that includes the sensible heat flux associated with rain, and the contribution of rain to the surface momentum flux. Using a mix of modeling and observations, three different case studies are examined in detail: clear and calm, clear and windy, and disturbed. For these typical sets of conditions and processes in the tropical ocean warm pool, the upper-ocean structure is clarified so that the skin sea surface temperature, the bulk surface temperature (at a depth of 1 cm), and the temperature at 0.5 and 5 m below the surface (which is the level that buoys and ships routinely observe "surface" temperature) can be interpreted. Sensitivity studies are conducted with the model to investigate the roles of wind speed, precipitation, ocean turbidity, and ocean initial state in modulating the radiation-induced diurnal cycle in SST. It is found that in high insolation, low wind regimes that the skin temperature may be as much as 30°C warmer than the 0.5-m buoy temperature. Spatial distribution of the diurnal amplitude of the SST are calculated for the global Tropics, and speculations are made regarding the implication of the SST variability to the tropical climate.

1. Introduction

In the tropical western Pacific Ocean (TWP), clouds and the cloud–radiation feedback can only be understood in the context of air–sea interactions and the ocean mixed layer. The importance of the TWP region to world climate has been described by Webster and Lukas (1992), among many others, and this region has been the focus of considerable research activity. To increase our understanding of the mean and transient states of the warm-water regions of the western Pacific Ocean and the associated air–sea interactions, the Tropical Ocean-Global Atmosphere (TOGA) Coupled Ocean–Atmosphere Response Experiment (COARE) program has been formulated (Webster and Lukas 1992). This program recently culminated in a major field experiment in the tropical western Pacific Ocean, with an intensive observing period (IOP) from November 1992 through March 1993. The Central Equatorial Pacific Experiment (CEPEX) was conducted during March 1993 to address specifically cloud–radiative feedback in the Tropics (Williams 1993). The Department of Energy Atmospheric Radiation (ARM) Program will continue this focus with long-term observations of clouds and radiation at a series of island sites in the TWP.

Considerable interest has been shown in attempting to explain why sea surface temperature (SST) rarely rises above 30°C, why the tropical western Pacific Ocean warm pool has relatively uniform SST between 28° and 30°C, and how clouds are related to the magnitude, variations, and gradients of the SST. Ramanathan and Collins (1991) postulated that cirrus clouds are the main mechanism that maintains the local SST at an equilibrium value in the tropical western Pacific. McPhaden and Hayes (1991), Wallace (1992), Fu et al. (1992), and Liu et al. (1994) have emphasized the importance of evaporation in regulating tropical SST, and McCreary and Lu (1994), Sun and Liu (1996), and Webster et al. (1996; manuscript submitted to *Science*) have described the role of ocean dynamics. Hartmann and Michelson (1993), Zhang (1993), Arking and Ziskin (1994), and Lau et al. (1994) emphasize the importance of large-scale atmospheric dynamics in cloud evolution over the warm pool, and thus in the regulation of warm pool SST.

Corresponding author address: Dr. Peter J. Webster, Program in Atmospheric and Oceanic Sciences, University of Colorado, Campus Box 311, Boulder, CO 80309-0429.

With the exception of the study by Fu et al. (1992), the observational studies have been conducted using monthly cloud and SST data, and the focus has been on intraseasonal and interannual timescales. The use of monthly averaged data misses a key feedback between clouds and SST that occurs on the fractional cloudiness-damping timescale of approximately 0.6 day and the cloud–SST coupling timescale, which was estimated to be 3–6 days for the unstable tropical atmosphere (Chu and Garwood 1991). This timescale is the time needed for a change in cloud properties, due to the change of ocean surface evaporation caused by SST variation, to feed back to the SST through its effect on the surface heat flux. The 3–6 day timescale was also found by Lau and Chan (1988) in a spectral analysis of the outgoing longwave radiation (OLR) over the equatorial western Pacific. A fractional cloudiness-damping timescale of approximately 0.6 day and an ocean mixed layer cooling timescale of approximately 20–30 days was also derived by Chu and Garwood (see also Webster 1994). The models described by Hu and Randall (1994) and Lau et al. (1994) are capable of addressing shorter timescale interactions between clouds and SST.

In the TWP, there are many scales and forms of convection, most of which reside within the 28°C surface temperature isopleth. Satellite-observed outgoing longwave radiation (OLR) estimates indicate that the TWP is dominated by deep and intense convection during most of the year. Early results from TOGA COARE indicate that the convective cloudiness is made up of a complicated menage of cloud life cycles. Smaller clouds and cloud clusters appear to undergo a distinct diurnal cycle (e.g., Mapes and Houze 1995). Larger mesoscale clusters are also tied to the diurnal cycle with a predawn maximum in convective activity, vertical extension, and precipitation. During the morning, the convective activity of these mesoscale clusters diminishes but cloudiness persists as extended stratus decks (Mapes and Houze 1995). Organized convection associated with disturbances may last for days. The larger-scale convection, in turn, appears to be modulated by a long period (30–60 day) dynamical pulse probably associated with large-scale ocean–atmosphere interaction (e.g., Lukas et al. 1995), which may in turn be modulated by the diurnal cycle in a cross-scale air–sea interaction scenario (Zhang 1996). Machado et al. (1992) and Machado and Rossow (1993) have noted that the frequency of tropical cloud clusters decreases as the inverse square of the radius of the disturbance, indicating in a statistical sense that the total area of deep cloud cover in the warm pool is approximately the same, irrespective of the scale of the components. Shallow convective clouds that have a small horizontal extent are abundantly present in this region, although they have not been studied systematically to date.

Different cloud types play different roles in the TWP climate. Deep convective precipitation accounts for approximately 40% of the total precipitation in the Tropics (e.g., Leary and Houze 1980; Liu et al. 1995), although these clouds cover a small area and thus have a relatively small impact on the radiation balance. Anvil clouds cover a much greater region and thus influence the radiation balance more strongly, while at the same time contributing approximately the same amount of total precipitation as do the deep convective clouds (e.g., Liu et al. 1995). Low- and midlevel clouds also modulate the surface radiation and freshwater fluxes. The type of cloud associated with the precipitation and the timing of this precipitation with respect to the diurnal cycle may influence the impact of the precipitation on the tropical sea surface temperature and ocean mixed layer characteristics, as initially suggested by Lukas (1991). Deep convective precipitation is typically associated with strong local surface winds, and the ensuing freshwater is easily mixed into the ocean below. By contrast, precipitation associated with shallow, isolated convection is generally accompanied by low wind speeds, resulting in the formation of a freshwater lens on the ocean surface that acts to stabilize the upper ocean and allows the sea surface temperature to warm radiatively (e.g., Webster and Lukas 1992).

To clarify the sea surface temperature, we must distinguish between the "skin" SST, which is the radiometric temperature of the sea surface, and the "bulk" sea surface temperature. The true bulk SST is defined to be the temperature within the upper few centimeters of the ocean surface. The bulk SST determined from buoy measurements is typically obtained at a depth of 0.5 m, while the bulk SST determined from ship measurements may be obtained from depths as deep as 5 m. We note that infrared wavelength measurements from satellites can be interpreted directly in terms of the skin temperature, although most methods of satellite SST retrieval have been regressed to reproduce bulk temperatures for comparison with in situ bulk temperature measurements made by ships and buoys (e.g., Reynolds and Marsico 1993). The radiative, latent, and sensible heat exchanges between the atmospheric and oceanic boundary layers depend on the actual skin temperature of the ocean, making the skin temperature the critical SST for examining air–sea interactions. The skin temperature can differ from the bulk water temperature in the Tropics by values that are as large as 1–3 K (e.g., Cechet 1993), although the magnitude of the bulk − skin temperature difference is usually <1 K (Schlussel et al. 1987, 1990; Wick et al. 1992; Coppin et al. 1991).

The mixed layer of the western equatorial Pacific Ocean has some unique features that make modeling the SST difficult. Lindstrom et al. (1987) have shown a more complicated structure to the warm-pool upper ocean than was previously thought. Rather than a deep isothermal layer surmounting a strong halocline, the near surface structure often contains a shallower isohaline layer accompanied by a warmer isothermal layer

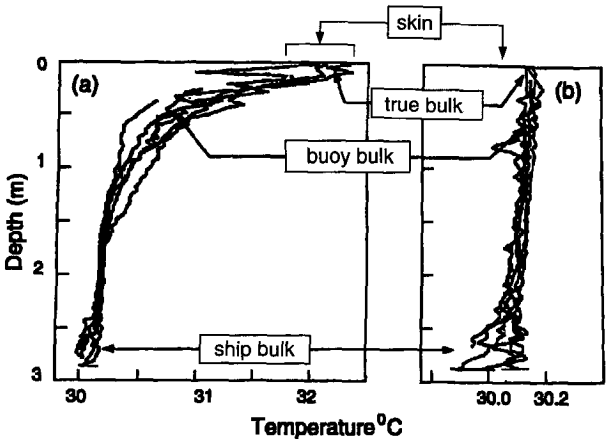

FIG. 1. Observations of temperature profiles in the ocean mixed layer obtained from the SILVERFISH instrument on board the R/V *Franklin* (a) 13 January 1993 and (b) 4 February 1993. The levels where the skin, true bulk, buoy bulk, and ship bulk SST values are commonly measured are indicated schematically in the diagram.

near the surface. This surface layer results from a strong freshwater flux into the ocean. Lukas and Lindstrom (1991) refer to the intermediate layer as a "barrier layer" that inhibits entrainment of colder, saltier water from below the main thermocline. Since surface winds in the western Pacific are generally light, the presence of the barrier layer effectively inhibits entrainment cooling. Lukas and Lindstrom (1991) concluded that the mixed layer in the western Pacific can only deepen significantly and cool when the winds are able to break through the barrier layer. Since strong enough winds to erode through the barrier layer are rare, a detailed knowledge of the role of surface fluxes is required to understand the SST.

Figure 1 shows observations of the upper-ocean temperature obtained from the R/V *Franklin* SILVERFISH (F. Bradley, personal communication) during the TOGA COARE Intensive Observation Period (IOP). Two different examples are given: Fig. 1a represents a case with light winds and high insolation, and Fig. 1b represents a disturbed situation with strong winds and low insolation. Profiles are shown for every 5 minutes over a period of 30 minutes. The different values of skin, true bulk, buoy bulk, and ship bulk "surface" temperatures are indicated schematically in the diagram. The skin SST was not measured coincidentally with these soundings, so the skin SST is represented schematically in the diagram based on model calculations to be approximately 0.4°C cooler than the 1-cm temperature during nighttime and approximately at the same temperature (or occasionally warmer) during daytime if surface insolation is high. A comparison of the two figures shows that in light wind conditions (Fig. 1a) very strong temperature gradients exist in the uppermost meter. In the disturbed case (Fig. 1b), the upper ocean is nearly isothermal and little diurnal variation is apparent. While the buoy (0.5 m) or ship (5 m) values of sea "surface" temperature are within a few tenths of a degree of the skin SST in Fig. 1b, the measurements obtained at the buoy or ship levels are several degrees cooler than the skin in Fig. 1a, even during the period of peak insolation.

To evaluate the interfacial fluxes of sensible and latent heat and the upwelling longwave radiation, the skin temperature of the surface of the ocean is the critical temperature. This temperature sets the saturation vapor pressure at the surface and so determines the latent heat flux into the atmosphere together with the atmospheric boundary-layer state. Thus, accurate values of the skin SST are required to determine accurate values of the surface heat flux components. Table 1 shows the changes in surface heat flux components associated with a 1°C change in SST for average conditions during the TOGA COARE IOP. The change in the upwelling longwave radiation flux at the surface was determined using the Stefan–Boltzmann law. To evaluate the changes in the sensible and latent heat fluxes, the bulk model described by Clayson et al. (1996) is used. Substantial changes are seen particularly in the surface latent heat flux. All of the changes are of the same sign, that is, none of the changes cancel if the net surface heat flux is being evaluated. Therefore, a 1°C change (or error) in sea surface skin temperature would result in a change (or error) of 27 W m^{-2} in the net surface heat flux. We note in particular that the percentage error in the turbulent flux will be even larger under conditions of lighter than average winds. In many instances, an error of this magnitude would be large enough to change even the sign of the net surface heat flux. An error of 20 W m^{-2} in moist static energy flux from the surface could significantly modify atmospheric boundary layer and convective processes. Because of the high surface temperatures and the Clausius–Clapeyron relationship, surface temperature variations (or errors) of magnitude 1°C can thus have substantial impact on air–sea interactions when the surface temperature is high. Ledvina et al. (1993) have pointed out the importance of using hourly values of bulk meteorological parameters in determining the daily average turbulent fluxes from bulk methods, showing that air–sea surface scalar fluxes computed from monthly, weekly, and even daily averaged bulk meteorological parameters can be seriously in error in equatorial, temporally variable wind

TABLE 1. Changes in surface heat flux components associated with a 1°C change in SST for average conditions during the TOGA COARE IOP.

Component	Flux change (W m^{-2})	Flux change (%)
Upwelling longwave	6.3	1.3
Sensible heat	2.4	23.3
Latent heat	18.7	16.2

regimes. Therefore, care must be taken in using the correct skin SST to evaluate the surface fluxes and in determining the diurnal variation of SST in the tropical western Pacific, which may be as high as 3.8°C under calm clear conditions (e.g., Fairall et al. 1996a).

In this paper, we use data obtained from the TOGA COARE IOP along with an ocean mixed layer model to address the relationship between clouds, surface radiation flux, and the sea surface temperature (SST) of the tropical western Pacific Ocean over the diurnal cycle, in the context of the Atmospheric Radiation Measurement (ARM) Program scientific objectives for the tropical western Pacific Ocean. The diurnal cycle encompasses a critical timescale for tropical air–sea interactions. Additionally, the TOGA COARE IOP dataset provides a large enough sample of diurnal cycles to address this topic systematically. A blending of the model and observations are used as this analysis would not be possible using only the observational data. Observations for the ocean mixed layer during the TOGA COARE IOP are presently available only once a day. Furthermore, there are no collocated observations of surface skin temperature. By examining the relationship between clouds, surface fluxes, and SST over the diurnal cycle we can interpret the details of the direct influence of clouds on SST. We examine the effects not only of the surface heat fluxes, but the freshwater and momentum fluxes as well. We also interpret these relationships in the context of the temperature variations at various depths in the ocean that are commonly used to describe "surface" temperature. Sensitivity studies are conducted with the model to investigate the roles of surface wind speed, precipitation, ocean turbidity, and ocean initial state in modulating the radiation-induced diurnal cycle in SST. We address the implications of a significant diurnal amplitude to the SST in regimes of light winds and high insolation. A simple parameterization is developed for the diurnal amplitude of the SST as a function of daily averaged wind speed, precipitation, and peak surface insolation. Spatial distributions of the diurnal amplitude of SST for the global Tropics is calculated and the question of whether these variations rectify to climate timescales is discussed.

2. TOGA COARE data

The TOGA COARE Intensive Observation Period (IOP) occurred from November 1992 through February 1993 in the western Pacific region bordered by 10°N, 10°S, 140°E, and 180°. Oceanographic and meteorological data were gathered from ships, buoys, aircraft, and satellites. A full overview of the TOGA COARE Intensive Observation Period (IOP), including the scientific goals of the program and the planned experimental design, is given by Webster and Lukas (1992), and details of the observational platforms are described by TOGA COARE IPO (1992).

In situ surface-based data obtained during the TOGA COARE IOP includes data from both buoys and research vessels. Shortwave and longwave radiation fluxes were measured from Eppley instruments on selected buoys. Some of the buoys were also equipped with optical raingauges so that freshwater flux estimates are available. These surface data are, in general, 1-hour averages of measurements made at various sampling rates. Subsurface data were also taken on all buoys, although the depth and resolution of the measured temperature, conductivity, and currents vary and only certain buoys measured the latter two quantities. Ocean temperature measurements were obtained from depths of 1 m to 4400 m (bottom). Salinity measurements, when obtained, were restricted to the upper 750 m of the ocean and current measurements were made between the surface and 1500 m.

Several datasets from research vessels are also available. In addition to the standard meteorological variables (temperature, humidity, winds, etc.), surface fluxes were measured. Measurements taken aboard the R/V *Moana Wave* (Fairall et al. 1996b) include the downwelling components of both shortwave and longwave radiation, which were also measured by standard Eppley pyranometers and pyrgeometers. Sea surface temperature (nominally at a depth of 1 cm) was measured using a thermistor sealed in the top of a floating hose. In order to measure the turbulent fluxes, mean and perturbation wind and temperature measurements were made using a sonic anemometer. A dual-wavelength infrared hygrometer was used to measure both mean and perturbation humidity. The turbulent fluxes were calculated using the direct covariance method, described by Fairall et al. (1990). Turbulent flux measurements are also available from both cruises of the R/V *Franklin* and the R/V *Malaita.* Each of the ships also carried instruments for measuring meteorological data that can be used for computation of bulk freshwater, heat, and momentum fluxes. Ocean microstructure measurements were also made aboard several of the research vessels, including the *Moana Wave,* the *Natsushima,* and the *Hakuho-Maru.*

In this study, we use the measurements obtained from the R/V *Moana Wave,* which provided a collocated dataset of surface fluxes and ocean microstructure measurements. The location of the *Moana Wave* during the measurements was 2°S, 156°E. Measurements were obtained during three separate periods: 11 November through 3 December 1992, 17 December 1992 through 12 January 1993, and 28 January through 16 February 1993.

A summary of the surface meteorology and surface fluxes from the R/V *Moana Wave* is given in Table 2; the maximum and minimum values presented are for hourly averages. Sea surface temperature (1 cm) shows a range of 6°C over the entire period. Surface wind speeds are relatively light but show a maximum value of 16 m s^{-1} during a westerly wind burst. Large variations are seen in the peak solar flux, associated with clouds, although clouds have much less influence on the surface longwave flux. Surface latent heat fluxes are

TABLE 2. Average values of surface parameters and fluxes measured by the R/V *Moana Wave* during the TOGA COARE IOP (surface flux is positive into the ocean).

Parameter	Average	Minimum	Maximum
SST, 1 cm (°C)	29.1	25.7	31.5
Wind speed, surface (m s^{-1})	4.9	0.1	15.9
Peak insolation (W m^{-2})	732.9	180.0	958.0
Longwave flux, down (W m^{-2})	413.0	370.0	441.0
Latent heat flux (W m^{-2})	−115.6	−7.0	−347.0
Sensible heat flux (W m^{-2})	−10.3	8.0	−69.0
Precipitation (mm h^{-1})	0.45	0	37.1

generally an order of magnitude larger than the sensible heat fluxes. Precipitation is very high in this region but occurs sporadically during the TOGA COARE IOP.

3. Model description

A variety of ocean mixed layer (OML) models have been used to study the tropical ocean mixed layer. These models may be grouped into roughly two categories: bulk and diffusion models. Bulk models attempt to model the OML in an integral sense (e.g., Kraus and Turner 1967; Garwood 1977; Price et al. 1986; Gaspar 1988). Diffusion models vertically resolve the OML and directly parameterize the turbulent mixing and diffusion in the OML (e.g., Mellor and Yamada 1982; Andre and Lacarrere 1985; Large et al. 1994; Kantha and Clayson 1994).

The 1D ocean mixed layer model that we use here is described by Kantha and Clayson (1994). The model uses second-order turbulence closure and incorporates the modified expansion of Galperin et al. (1988) that leads to a much simpler and more robust quasi-equilibrium turbulence model than the original Mellor and Yamada (1974) formulation. Improvements have also been made to the parameterization of the pressure covariance terms in the second-moment closure, based on results from large-eddy simulations. Penetration of shortwave radiation into the upper ocean is modeled following Morel and Antoine (1994) using three spectral intervals. This level of complexity is necessary, as Woods et al. (1984) and Lewis et al. (1990) have shown that shortwave radiation penetrates to a significant degree below the upper mixed layer of the ocean. Treatment of the shear instability-induced mixing in the strongly stratified region below the oceanic mixed layer is done following Large et al. (1994). It may be questioned whether one-dimensional mixed layer models can perform adequately in the equatorial regions because of the strong advective and other 3D processes in the equatorial waveguide. However, it was shown by Kantha and Clayson (1994) that the 1D model (with the parameterization for shear-instability-induced mixing) can be used for time periods on the order of a week close to the equator. The model has been validated over many timescales and in many locations, including data from the TOGA COARE Pilot Cruise (Kantha and Clayson 1994).

A parameterization for skin SST has been added to the Kantha–Clayson model. Based on surface renewal theory, Liu et al. (1979) showed that the temperature difference ΔT between the ocean skin and bulk temperatures should be related to the net surface heat flux (Q_N), surface friction velocity (U^*), and the surface roughness Reynolds number (Re). This theory has been extended by Soloviev and Schlüssel (1994), who determined the following for the temperature difference between the ocean skin and bulk temperatures:

$$\Delta T \alpha \frac{Q_N}{\rho_w c_p} \left(\frac{t_r}{\kappa} \right)^{1/2}, \tag{1}$$

where Q_N is the net surface heat flux, ρ_w is the density of seawater, c_p is the specific heat of seawater, κ is the coefficient of thermal diffusion of seawater; t_r, the time period over which eddies are renewed, is given by Wick (1995):

$$t_r = t_{rs} + (t_{rc} - t_{rs}) \exp(R_{fcr}/R_{f0}), \tag{2}$$

where t_{rs} and t_{rc} are respectively the timescales for surface renewal due to viscous stress variations and due to cyclic injections of fluid from the molecular sublayer of a convective nature. The surface Richardson number controls the transition from free to forced convection in the near surface water. Further details on this parameterization are described by Soloviev and Schlüssel (1994) and Wick (1995), including validation of the parameterization. Soloviev and Schlüssel (1996) have examined the evolution of the cool skin during daytime. During the daytime, absorption of solar radiation within the thermal molecular sublayer of the ocean can modify the temperature difference across the cool skin. Under low wind speed conditions, the solar heating damp the convective instability, strongly increasing the renewal time. During strong insolation, the skin temperature may be warmer than the true bulk temperature defined in Fig. 1. Under low wind conditions, convective instability caused by salinity flux due to evaporation limits the surface temperature increase. A skin SST parameterization has been incorporated into the Kantha and Clayson (1994) ocean mixed layer model, following Soloviev and Schlüssel (1994, 1996) and Wick (1995). When it is raining heavily, the ocean skin is influenced by the water and momentum flux associated with the rain. Calculations (P. Schlüssel, personal communication) indicate that this effect on the skin temperature is relatively small unless rainfall rates are very heavy.

The surface fluxes of radiation, sensible and latent heat, fresh water, and momentum are specified using hourly values measured on the *Moana Wave* (following Young et al. 1992). Also included are additional surface fluxes associated with precipitation. The surface

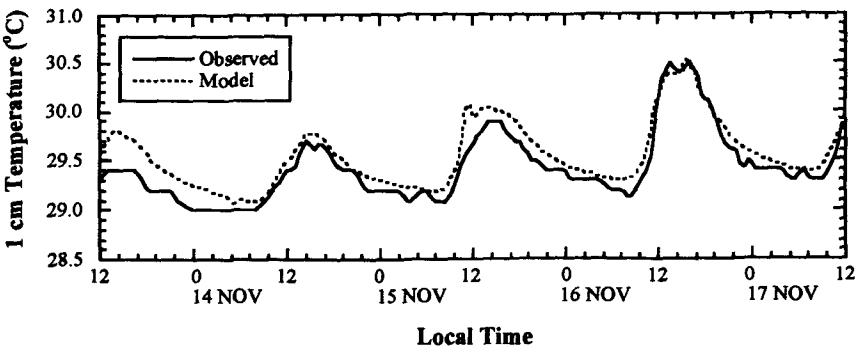

FIG. 2. Time series comparison of modeled with observed 1-cm temperature for the 4-day simulation for case 1 (Table 3).

momentum flux associated with rain is included following Kantha and Clayson (1994), based on the parameterization described by Caldwell and Elliot (1971). The surface sensible heat flux associated with rain is parameterized following Gosnell et al. (1995).

A vertical resolution of 1 m was used in the model simulations, with an additional model level at 1 cm below the surface. A time step of 15 minutes was used in the model integrations. The average pressure gradient and equatorial undercurrent characteristics used in these sensitivity studies are specified using the analyses of Leetmaa and Ji (1989) for the TOGA COARE IOP. The use of the average pressure gradient is justified for such short timescales simply because the equatorial ocean is never in equilibrium on these scales.

The model is forced at the upper boundary by observed surface flux measurements obtained from the *Moana Wave* (made available by C. Fairall) with a time interval of 15 minutes. The OML model is initialized using the ocean microturbulence measurements obtained from the *Moana Wave* (made available by M. Gregg). These measurements are presently available once per day (at noon), at a vertical resolution of 1 m. No ocean microturbulence measurements are reported above 2 m, although a temperature measurement is made at a depth of approximately 1 cm by the floating thermistor. It is therefore difficult to initialize the model in the upper 2 m, especially at noon when the upper-ocean temperature structure is complicated by the absorption of shortwave radiation. The model is therefore initialized in the upper 2 m using the 1 cm and uppermost microturbulence measurement with an appropriate exponential solar heating profile. The model is then run for a total of 4 days, allowing the upper-ocean temperature and salinity to adjust to the surface forcing.

An example of the model "spinup" is shown in Fig. 2, where the modeled and observed 1-cm ocean temperatures are compared for case 1 (see Table 3). The observed and modeled nocturnal temperatures are fairly close, but large differences between the peak

TABLE 3. Summary of case study statistics. Dates correspond to a 24-h period beginning at midnight of the previous day and ending at midnight on the specified date.

	Case						
	1	2	3	4	5	6	7
Date (mo/d)	11/16	11/23	12/26	12/31	1/0	2/3	2/9
Peak insolation (W m^{-2})	929	368	629	857	910	852	557
Average wind speed (m s^{-1})	2.7	6.0	5.5	9.5	1.8	5.3	4.9
Total precipitation (mm)	3.3	6.9	70.5	2.2	0.2	10.3	51.4
Average temperature (K)							
Skin	29.47	28.87	28.56	28.36	29.03	28.86	28.80
Bulk	29.66	29.08	28.80	28.62	29.21	29.08	29.02
0.5 m	29.61	29.09	28.83	28.64	29.33	29.10	29.03
5.0 m	29.44	29.10	28.89	28.65	29.13	29.08	29.05
Diurnal temperature range (K)							
Skin	1.21	0.03	0.18	0.13	1.56	0.44	0.03
Bulk	1.22	−0.05	0.35	0.12	1.55	0.42	0.05
0.5 m	0.92	−0.06	0.28	0.10	1.00	0.36	0.05
5.0 m	0.31	−0.06	0.11	0.07	0.23	0.24	0.03
Average OML depth (m)	4.9	31.1	13.0	34.6	4.7	28.8	23.6

noontime temperatures are seen, with the modeled peak temperature 0.6°C warmer than observed after 24 hours of integration. After the fourth day of integration, the model shows very good agreement with the observations. Figure 3 compares the modeled profiles of temperature and salinity at noon of the fourth day of integration. Observations and simulations match rather well, with the model reproducing much of the fine structure in the thermal and salinity profiles of the upper ocean.

4. Diurnal cycle

The joint time series of SST, ocean mixed layer characteristics, surface heat flux components, surface wind speed, and rainfall rate are now examined using a blend of observations and model calculations. Surface flux components at 10-minute time resolution determined from measurements made on the R/V *Moana Wave* are used. Only the true bulk surface temperature (1 cm) is available at this resolution; coincident values of the skin, 0.5-m bulk and 5.0-m bulk SST are determined using the ocean mixed layer model, forced by surface fluxes every 15 minutes. We note, once again, that this analysis would not be possible using only the observational data because observations for the ocean mixed layer are presently available only once a day and because there are no collocated observations of skin temperature. In this analysis, we consider data and model calculations for the fourth day of a four-day model integration (see section 3). The root-mean-square error of the modeled 1-cm temperature relative to the observed value was in all cases less than 0.1°C during the fourth day of integration, which is smaller than the stated accuracy for the thermometer. The only situations where the modeled 1-cm temperature did not show good agreement with the observations was for situations where the wind speed exceeded 10 m s^{-1} and the instantaneous observed temperature differed by more than 1°C from preceding and following measurements; we infer that under these conditions the floating thermistor is not maintained at 1-cm depth and thus the comparison with observations is inappropriate.

Table 3 presents a summary of seven cases representing a range of conditions encountered, for which we could obtain a reasonably homogeneous 4-day time series (as determined by the surface fluxes). The data presented in Table 3 correspond to the last 24 hours of a 4-day run that began at local midnight on the specified date. The diurnal temperature variability is determined by comparing the noon maximum with the predawn minimum during that 24-hour period. The ocean mixed layer depth was determined from the depth at which the modeled surface-forced turbulence kinetic energy becomes nearly zero. The difference between the daily average skin and bulk SST (1 cm) is seen to range between 0.2° and 0.3°C, with the skin cooler than the true bulk SST in terms of the average values. Differences between the daily average skin SST and the buoy (0.5 m) and ship (5.0 m) bulk SST range from 0.14° to 0.3°C. Nearly clear-sky conditions were present for cases 1, 4, and 5; isolated clouds were present for cases 3 and 6; and cases 2 and 7 represent disturbed conditions. Table 3 shows that there is no strong correlation between the daily peak insolation and average skin SST. The diurnal temperature range was determined by the skin SST difference between the predawn minimum and the maximum value that occurs shortly after the

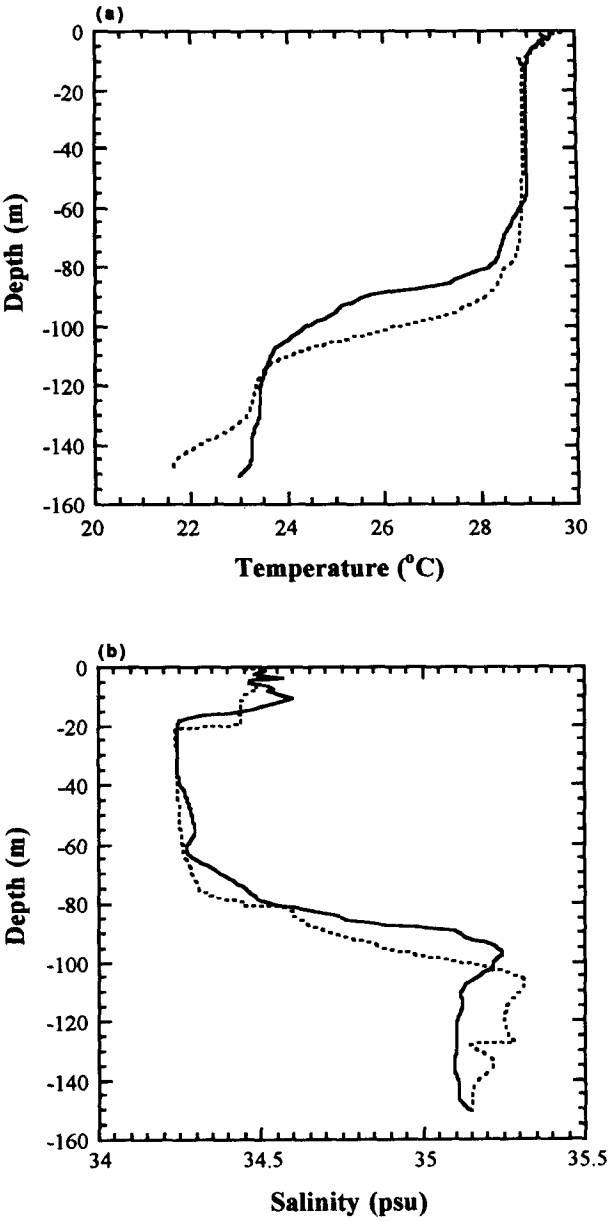

FIG. 3. Profiles of modeled and observed (a) ocean temperature and (b) salinity at noon on date representing the fourth day of model integration for case 1 (Table 3).

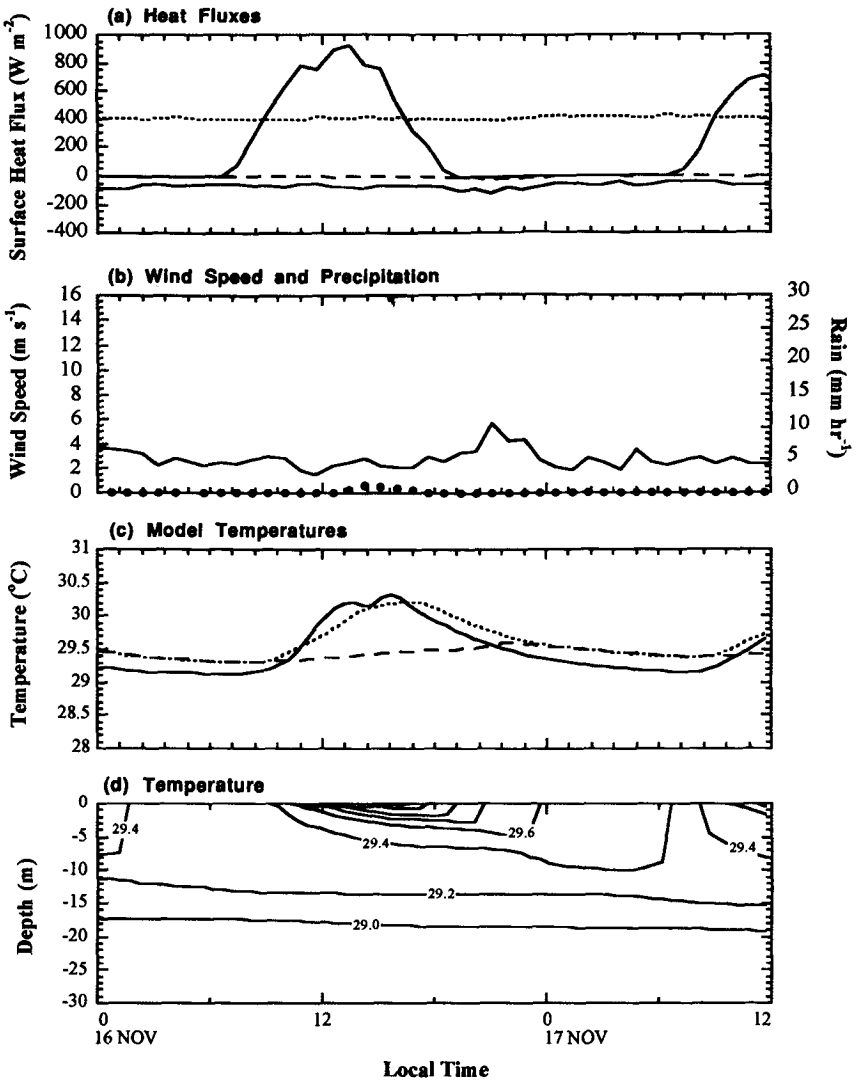

FIG. 4. Time series corresponding to the last 36 hours of model results for case 1: (a) observed surface fluxes of shortwave (solid), longwave (dot), sensible (dash), and latent heat (solid: negative values) fluxes; (b) observed surface wind speed (solid) and rainfall rate (closed circles); (c) skin SST (solid), 0.5-m temperature (dot), and 4.5-m temperature (dash); (d) time–height cross section of upper-ocean temperatures.

peak insolation. The negative values of diurnal temperature range shown in Table 3 for cases 2 and 7 reflect the general absence of a diurnal cycle and an overall cooling of the SST. The highest values of skin SST and greatest diurnal range in skin SST occur for cases 1 and 5. These two cases have the lowest wind speeds and the shallowest mixed layer depths. The shallow mixed layer depth increases the response of the mixed layer temperature to surface heating. Cases 3 and 4 occur just after a westerly wind burst and are accompanied by high wind speeds and a deepened ocean mixed layer, resulting in a very low diurnal range in skin SST, even though the peak insolation for case 4 is fairly high.

Detailed case studies for three different situations are described below: clear and calm (case 1), clear and windy (case 4), and disturbed (case 7).

a. Case 1: Clear and calm

Case 1 began on 14 November 1992 and is characterized by clear skies, high insolation, and low wind speeds (see Table 3). The time series associated with the last 36 hours of model integration (17 November) of the observed surface fluxes and wind speed are shown in Figs. 4a–b. A few isolated clouds are indicated by slight depressions in the solar radiation flux,

but the peak insolation exceeds 900 W m^{-2} on all four days. Very little precipitation occurred during this period. Surface wind speeds were low, with an average and peak wind speed of 3 and 6 m s^{-1}, respectively. Figure 4d shows the time–height cross section of ocean temperature down to a depth of 30 m. As determined from the ocean turbulence cross section (not shown), an average mixed layer depth of 4.9 m is determined for this period.

Figure 4c compares several different "surface" temperatures. The skin SST is always cooler than the bulk SST determined at 1-cm depth (not shown) and varies by a maximum difference of 0.24°C at night to a minimum of 0.14°C during the peak insolation period. The skin SST is cooler by 0.2°C on average than the 0.5-m temperature during the night but becomes warmer by nearly 0.3°C near noon. Averaged over one diurnal cycle, the average 1-cm bulk temperature is 29.7°C, with the average 0.5-m (buoy) and 5.0-m (ship) temperatures being 29.6° and 29.4°C, respectively. Although there is only a few tenths of a degree difference between the different determinations of the daily mean "surface" temperature, there are large differences in the amplitude of the diurnal surface temperature range, from 0.31°C at a depth of 5.0 m to 1.22°C at a depth of 1 cm. Additionally, Figs. 4c–d show that there is a phase lag with depth of the diurnal cycle. The peak heating at 4.5-m depth occurs approximately 7 hours after the maximum value of skin SST. At the time of peak insolation, the mixed layer is above 5.0 m. The daytime heating is only reflected at depths greater than 4 m following the nocturnal deepening of the mixed layer.

b. Case 4: Clear and windy

Case 4 commenced on 29 December 1992 and was characterized by clear skies, high insolation, and relatively high wind speeds (see Table 3). The time series associated with the last 36 hours of model integration (31 December to 1 January) of the observed surface fluxes and wind speed are shown in Figs. 5a,b. A few isolated clouds are indicated by slight depressions in the solar radiation flux, especially on day 3, but the peak insolation remained above 850 W m^{-2} for each of the days during this period. Several small precipitation events are evident in Fig. 5b. Surface wind speeds were high, with an average and peak wind speed of 9.5 and 12 m s^{-1}, respectively. Figure 5d shows the time–height cross section of ocean temperature down to a depth of 30 m. As determined from the ocean turbulence cross section (not shown), the average mixed layer depth was 34.6 m. This case occurred during a westerly wind burst, which was accompanied by a substantial deepening of the ocean mixed layer.

Figure 5c compares the different "surface" temperatures. The skin SST is seen to be 0.26°C cooler than the SST determined at 0.5-m depth with only small variations throughout the diurnal cycle. The average 1-cm bulk temperature is nearly equal to the 0.5- and 5.0-m temperatures at 28.6°C, with the diurnal amplitude ranging from 0.13°C for the skin SST to 0.07°C for the 5.0-m temperature.

A comparison of this case with case 1 illustrates the importance of wind speed and ocean mixed layer depth on sea surface temperature under clear-sky conditions. The deeper ocean mixed layer and increased evaporative cooling result in lower surface temperatures, a reduced diurnal amplitude in SST, and a reduced phase lag of temperature with depth.

c. Case 7: Disturbed

Case 7 commenced on 9 February 1993 and was characterized by cloudy skies, low insolation, and intermediate wind speeds (see Table 3). The time series associated with the last 36 hours of model integration (11 February) of the observed surface fluxes and wind speed are shown in Figs. 6a,b. Clouds were present during the entire period, with the peak daily insolation dropping as low as 442 W m^{-2}. Significant amounts of precipitation occurred during this period. Surface wind speeds were intermediate, with an average and peak wind speed of 4.4 and 11 m s^{-1}, respectively.

Figure 6c compares the different "surface" temperatures. The skin SST is again seen to be on average 0.18°C cooler than the bulk SST determined at 1-cm depth (not shown) and the 0.5-m temperature but varies between 0.3°C and 0.1°C throughout the diurnal cycle. A slight surface cooling immediately following the two large precipitation events during this period is apparent. The temperatures at 0.5 and 5.0 m show very little change, although a slight cooling following the precipitation events is apparent at these depths as well.

A comparison with case 4 illustrates the importance of clouds and precipitation on the diurnal cycle of the skin SST. The diurnal amplitude of the SST is substantially reduced by the presence of clouds. The effects of short-lived wind and precipitation events have an impact on the skin and true bulk SST but less influence on the temperatures at depth.

5. Sensitivity studies

Simple correlations between variables is not sufficient to reveal causality. As pointed out by Stephens and Slingo (1992), it is difficult to separate cause and effect and to isolate the feedback mechanisms between the atmosphere and SST using observational data. This is especially true for a complicated, nonlinear system such as the upper ocean. Therefore, diagnostic studies cannot unambiguously identify feedbacks. However, carefully designed model experiments can be used to quantify the relative importance of different physical processes and to isolate causal mechanisms, provided that the models accurately simulate the relevant climate

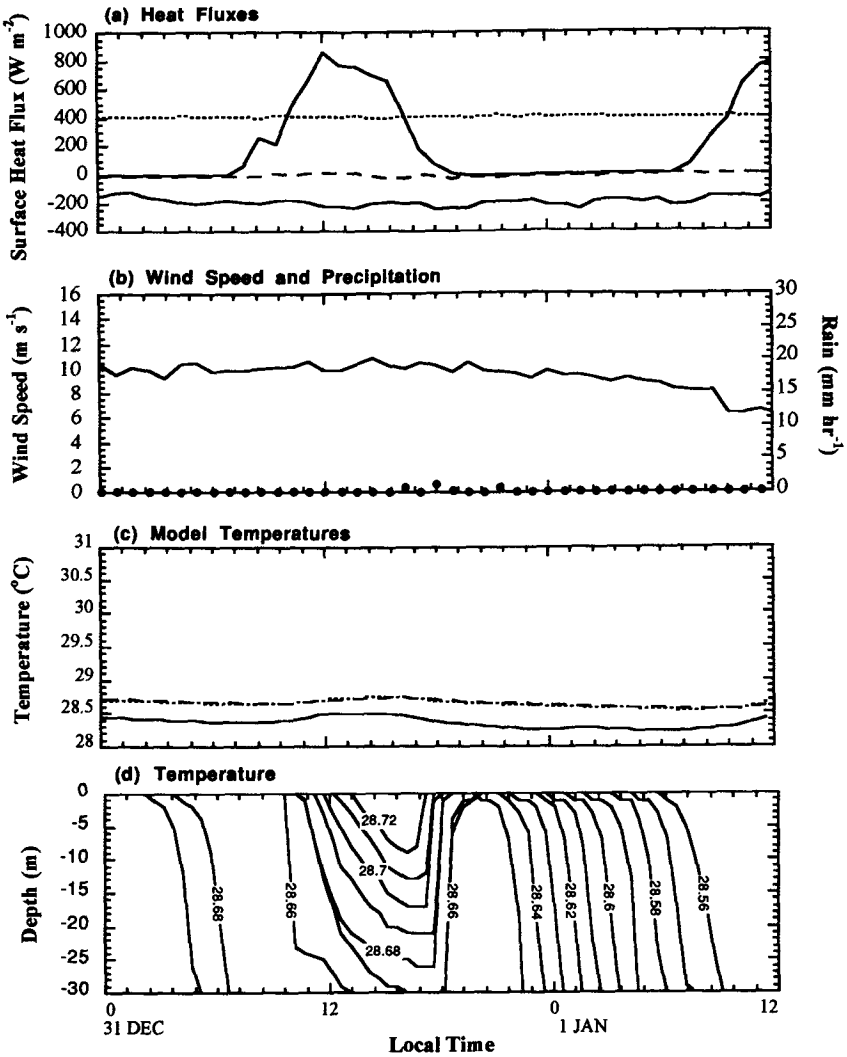

FIG. 5. Time series corresponding to the last 36 hours of model results for case 4 (following Fig. 4).

processes and sensitivities. The Kantha and Clayson (1994) OML model is now used to explore some of the characteristics of the relationships between solar radiation, wind speed, and precipitation in influencing the diurnal SST variability.

The model is initialized with average ocean conditions for the TOGA COARE period. A number of experiments were run to assess the sensitivity of the diurnal amplitude in SST to the initial profile of temperature and salinity in the ocean and the depth of the mixed layer. An evolving ocean mixed layer will certainly have an influence on the SST, and a deepening OML will have a cooling effect on SST as cold water from below is entrained into the mixed layer. However, whereas the effect of the ocean initial conditions on the absolute SST is important, the effect on the diurnal amplitude of the skin SST is relatively small.

The model is again integrated for a period of four days. The results are presented for the diurnal cycle of the last day of the integration unless otherwise specified. The results shown below focus on the skin SST and the 0.5-m temperature.

a. Solar radiation

Solar radiation is responsible for the diurnal cycle in SST and surface solar radiation flux is modulated primarily by cloud characteristics. Because of the opacity of the tropical atmosphere in the infrared due to the high water vapor content in the lower atmosphere, clouds have very little impact on the surface longwave flux (e.g., Stephens and Webster 1979; Webster 1994). Therefore, variations in the surface solar radiation flux are an excellent proxy for changes in cloud characteristics.

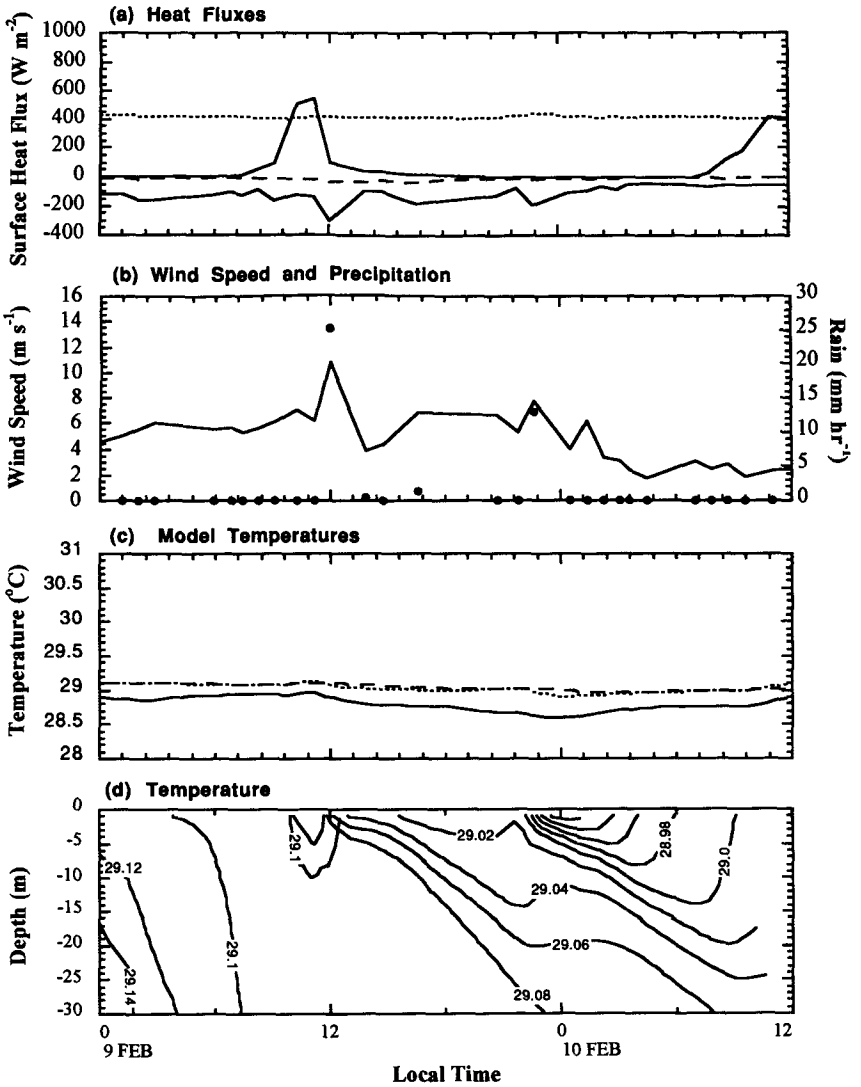

FIG. 6. Time series corresponding to the last 36 hours of model results for case 7 (following Fig. 4).

Figure 7 illustrates the magnitude of the diurnal cycle of skin SST for varying magnitudes of surface insolation for a constant wind speed of 3 m s^{-1}. The surface insolation is represented by the peak value of the noontime solar insolation, effectively assuming a steady cloud cover over the diurnal cycle. The diurnal SST cycle is represented by the change in SST relative to the pre-sunrise skin temperature (the diurnal cycle evolves clockwise from the lower left-hand corner of the diagram). The pattern of the diurnal cycle in the insolation versus SST plot shows a surface temperature increase that follows the surface insolation, with SST still increasing several hours after the peak insolation. As expected, the amplitude of the diurnal cycle is largest for the largest insolation, the amplitude of the diurnal cycle being virtually zero for peak insolation values less than 300 W m^{-2}. Although the amplitude of the diurnal cycle is diminished with increasing wind speed (see section b below), the general trend remains the same for varying solar insolation at higher wind speeds.

Comparison of the diurnal amplitude of the skin SST (Fig. 7a) with that of the 0.5-m temperature (Fig. 7b) shows that the diurnal amplitude at 0.5 m follows the same general pattern as the skin SST. However, the amplitude of diurnal cycle at 0.5 m is reduced by approximately 25% relative to the skin SST.

b. Surface wind speed

Surface wind speed modulates the amplitude of the diurnal cycle by influencing the surface heat flux (through the sensible and latent heat flux) and by deter-

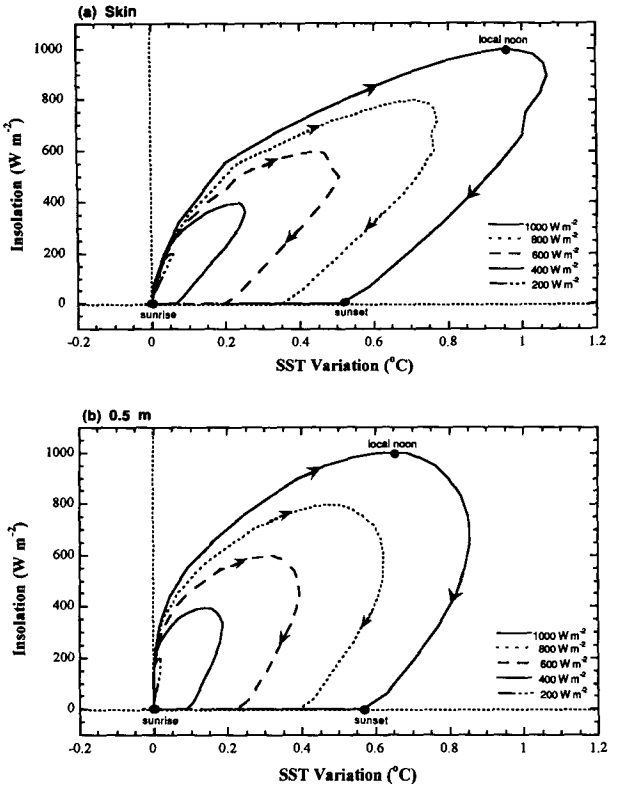

FIG. 7. The evolution of the skin SST over the diurnal cycle, plotting solar insolation versus the change of skin SST relative to the pre-sunrise skin temperature, for varying values of peak solar insolation (surface wind speed 3 m s^{-1}, no precipitation). (a) Skin SST; (b) 0.5-m temperature.

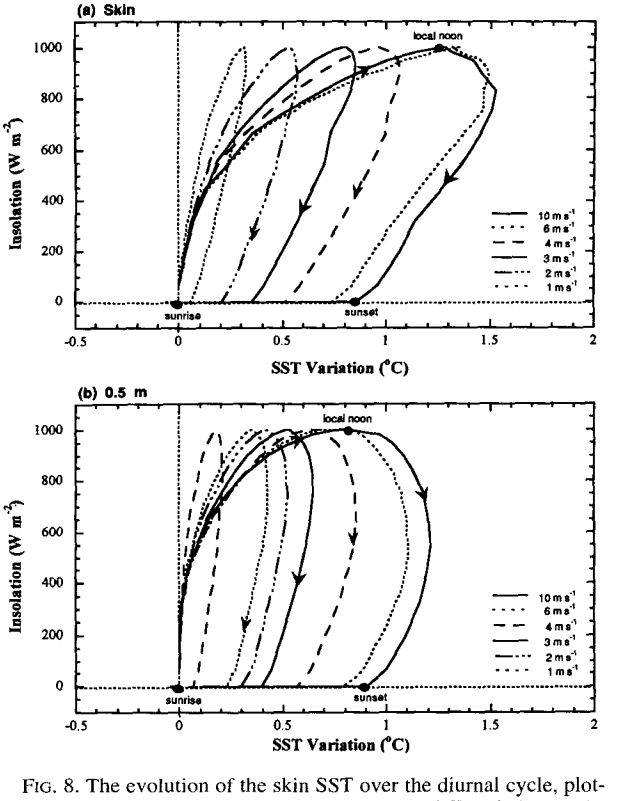

FIG. 8. The evolution of the skin SST over the diurnal cycle, plotting solar insolation versus the change of skin SST relative to the pre-sunrise skin temperature (peak surface insolation 900 W m^{-2}, no precipitation). (a) Skin SST; (b) 0.5-m temperature.

mining the momentum flux. In general, wind speed is negatively correlated with sea surface temperature, with increased wind speeds increasing the net surface heat flux and increasing the upper ocean mixing, thus distributing the surface heating throughout a greater depth of the ocean and diminishing the surface warming.

Figure 8 compares the diurnal amplitude of the surface temperature (skin SST and 0.5 m) for varying surface wind speeds, for a peak insolation of 1000 W m^{-2}. The range of wind speeds chosen here spans the range of average daily wind speed encountered during the IOP. Using the bulk surface turbulence flux parameterization described by Clayson et al. (1996), we determined variations in surface sensible and latent heat fluxes with varying surface wind speed. Figure 8 shows the values of the diurnal SST amplitude for varying wind speeds, including the influence of the surface wind on both the surface momentum and the latent and sensible heat fluxes. As expected, the diurnal amplitude of the surface temperature decreases with increasing wind speed. However, the diurnal amplitude of SST does not change linearly with wind speed. At the high end of the wind speed range, the diurnal amplitude of SST is much less sensitive to changes in wind speed than at the lower end of the wind speed range. An analogous set of experiments was run for a peak insolation of 500 W m^{-2}, showing a similar trend for varying surface wind speed, although overall the diurnal amplitudes were considerably smaller, as expected from the results of Fig. 7. As was seen in Fig. 7, the magnitude of the diurnal amplitude is about 25% smaller at 0.5 m relative to the skin.

The nonlinearity in the diurnal amplitude of SST can be interpreted by examining the OML depth associated with the different wind speeds, shown in Table 4. The

TABLE 4. Values of ocean mixed layer depth for variations in surface momentum flux (corresponding to Fig. 8).

Wind speed (m s^{-1})	Mixed layer depth (m)
1	2.3
2	2.9
3	4.4
4	6.1
5	7.1
6	8.1
10	11.3

decreased diurnal amplitude at high wind speeds arises from the increase in mixed layer depth.

c. *Precipitation*

The effects of precipitation on SST are complex since precipitation influences the surface fluxes of heat, freshwater, and momentum. Precipitation results in a decrease in surface salinity, a cooling of the surface [since the temperature of the rain is effectively at the wet-bulb temperature of the atmosphere above the surface, e.g., Gosnell et al. (1995)], and an increased mixing.

The freshening and cooling associated with precipitation have opposing effects on the ocean surface buoyancy flux. The ocean surface buoyancy flux may be written as

$$B = c_w^{-1} g \alpha Q_N + g\beta(E - P)S, \qquad (3)$$

where Q_N is the net surface heat flux, E is the evaporative flux of water, P is the precipitation, c_w is the specific heat of sea water, g is the gravitational acceleration, S is the salinity, and α and β are respectively the expansion coefficients associated with temperature and salinity. Using the expression for the sensible heat flux associated with precipitation, Q_p (following Gosnell et al. 1995),

$$Q_p = c_w(\mathrm{SST} - T_{\mathrm{wa}})P, \qquad (4)$$

where T_{wa} is the atmospheric wet-bulb temperature, we may evaluate the ratio of the heating to salinity effects as

$$\frac{\alpha(\mathrm{SST} - T_{\mathrm{wa}})}{\beta S} = 0.1, \qquad (5)$$

where standard values of the coefficients appropriate to the tropical ocean surface and an average value of SST $- T_{\mathrm{wa}} = 4.7$°C were used. It is seen from (5) that the freshening effect of rain dominates over the cooling effect in terms of ocean surface buoyancy flux, although the sensible heat flux of rain (which is typically neglected) is an important contribution to the surface buoyancy flux.

Figure 9 illustrates the impact of varying rainfall amounts on the diurnal cycle of skin SST (Fig. 9a) and 0.5-m temperature (Fig. 9b) for a peak insolation of 500 W m^{-2} and constant wind speed of 3 m s^{-1}. In these simulations, the rainfall begins after 72 hours and continues at a constant rate for the remainder of the 4-day period; the last 24 hours are shown in Fig. 9. The magnitude of the diurnal SST amplitude is not influenced by rainfall rates less than 0.5 mm h^{-1}; for the specified wind speed, small amounts of freshwater are rapidly mixed downward. At larger rainfall rates, the diurnal amplitude of SST increases as the formation of a fresh and stable layer at the surface allows greater surface heating. For higher wind speeds, the diurnal amplitudes are much smaller and much less influenced

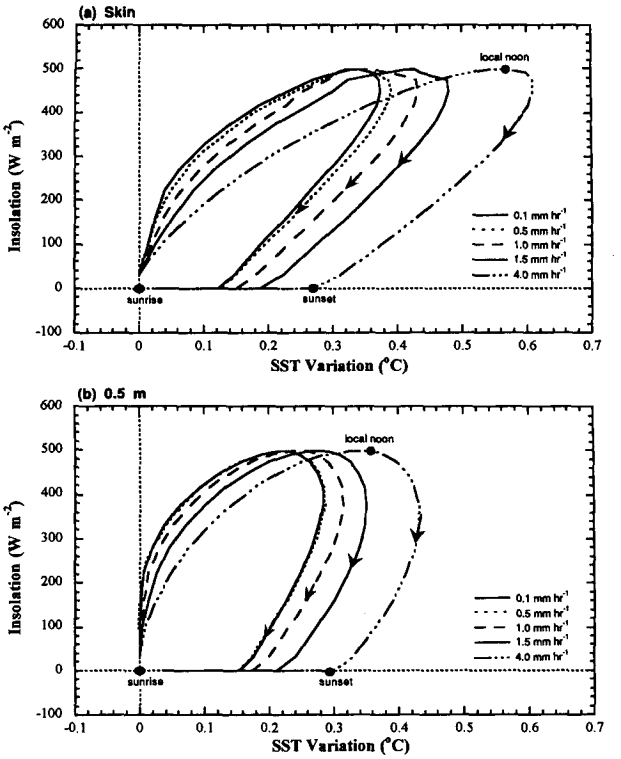

FIG. 9. The evolution of the skin SST over the diurnal cycle, plotting solar insolation versus the change of skin SST relative to the pre-sunrise skin temperature, for varying precipitation rates that are constant over the diurnal cycle (peak surface insolation 500 W m^{-2}, wind speed 3 m s^{-1}). (a) Skin SST; (b) 0.5-m temperature.

by precipitation due to increased mixing of the fresh water throughout the upper layer.

Furthermore, the impact of precipitation may depend on when the precipitation occurs in the diurnal cycle. Figure 10 shows a time series of the deviation of SST from the predawn minimum value over a 36-hour period. In all of the precipitating cases, the total amount of rainfall is the same (80 mm) but its distribution over the diurnal cycle is different. In Fig. 10, morning (AM) rain fell between 0800 and 1000 (local time), afternoon (PM) rain fell between 1400 and 1600, and night (N) rain fell between 2100 and 2300. Relative to the constant rain case, the AM rain case is warmer in the afternoon and cooler the following night; the PM rain is cooler throughout the diurnal cycle; and the N rain is significantly cooler during the period after the rainfall. At 0500 of the day following the rainfall, the coldest SST is for the N rain, and the warmest skin SST is for the constant rain. During each case where there was a short period of rainfall, the skin SST decreased during the rain event due to the sensible heat associated with the cooler rain mass. However, depending upon the time of day, this cooler but fresher stable layer increased in temperature faster than the warmer but deeper layer due to decreased mixing of the heat down-

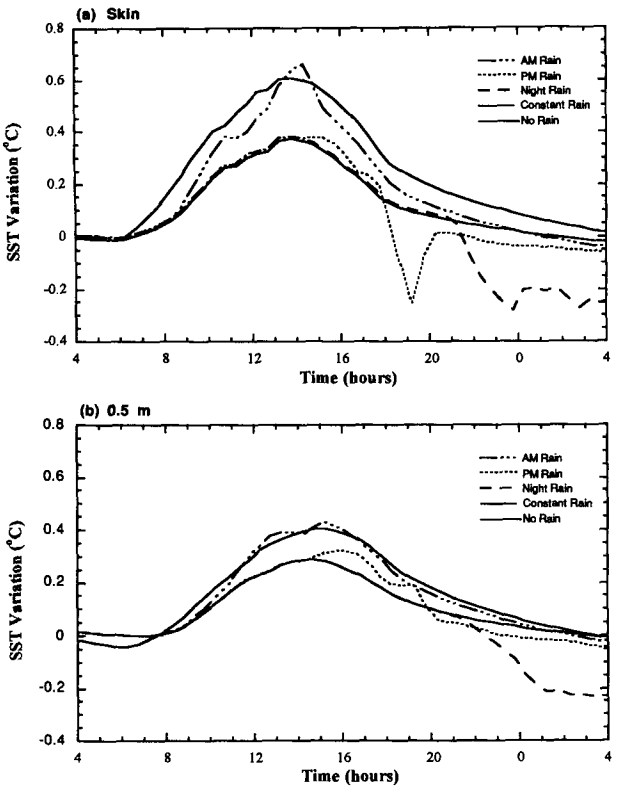

FIG. 10. Time series plot of deviation of SST from the predawn value for different temporal distributions of 80 mm of rain.

ward. Thus, the AM rain is initially associated with a cooler skin SST than the other cases but ends up warmest due to enhanced heating of the fresh layer throughout the day. At 0.5 m (Fig. 10b), similar trends occur to those found at the skin, although the differences between each of the precipitation cases (except for the N rain) is greatly reduced.

d. Summary

The magnitude of the diurnal SST amplitude for varying surface forcing is summarized in Fig. 11, where variations are examined for peak insolation, wind speed, and rainfall rate for average conditions of the ocean mixed layer during TOGA COARE. As determined from Figs. 7–9, the magnitude of the diurnal variation of the SST increases with increasing insolation, decreases with increasing wind speed, and increases with increasing amounts of precipitation. For peak insolation values of less than 200 W m^{-2}, the diurnal amplitude is near zero or slightly less than zero for all values of wind speed and precipitation that were considered, except for the combination of the lowest wind speed and the highest precipitation. Increasing wind speed diminishes the impact of precipitation on the diurnal SST amplitude. At wind speeds $\geq$ 10 m s^{-1}, the diurnal amplitude is effectively zero, independent of insolation and precipitation values. It is clear from Fig. 11 that the diurnal amplitude of the SST is very nonlinear. In general, for a given wind speed, the diurnal amplitude of the SST increases as a function of rainfall rate. This may be seen clearly in Fig. 10. However, as wind speed decreases below about 2 m s^{-1}, the amplitude becomes almost independent of precipitation. The reason for this is as follows: Generally, the heating that occurs in near surface is a function of two competing processes: radiative heating and turbulent mixing. Precipitation tends to minimize mixing by creating a stable near surface layer. However, for very low wind speeds there is little wind mixing and the heating rate of the upper ocean approaches the limit defined by the radiative attenuation characteristics of the upper ocean. Thus, in the very low wind regime increased stabilization of the surface layer becomes irrelevant. In other words, the upper layer of the ocean cannot heat any more for a given peak insolation.

The results shown in Fig. 11 can be used to develop a parameterization of the diurnal amplitude of skin SST (dSST) that depends on the magnitude of the peak solar insolation, the cumulative amount of daily precipitation, and the average daily wind speed. A regression equation relating diurnal SST variability to peak solar insolation, daily average precipitation, and daily average wind speed is determined to have the following form:

$$\mathrm{dSST} = f + a(\mathrm{PS}) + b(P) + c\ln(U) + d(\mathrm{PS})\ln(U) + e(U), \quad (6)$$

where the peak solar insolation (PS) is in watts per square meter, the daily averaged precipitation (P) is in millimeters per hour, and the 10-m wind speed (U) is in meters per second. The coefficients are presented in Table 5, where different coefficients are determined for $U > 2$ m s^{-1} and $U \leq 2$ m s^{-1}. The overall bias of this parameterization is less than 0.05°C, with a maximum bias at very high wind speeds of 0.07°C.

The results of this study imply that the normal specification of sea surface temperature for the NOAA operational SST dataset that is used in numerical weather prediction models and climate simulations (using either atmospheric or oceanic models) can lead to errors in the modeled surface fluxes that arise because skin SST is not used in the calculations and the diurnal amplitude in skin SST is omitted.

To gauge the magnitude of amplitude of the diurnal variation in SST to the values of SST used in numerical weather prediction models, we examine a single day from the ECMWF initialized analyses, 1 April 1988. The ECMWF model utilizes weekly values of bulk SST obtained from the NOAA operational SST dataset as its lower boundary condition. Figure 12c shows a map of the bulk sea surface temperature in the tropical Pacific and Indian Oceans for the week of 1 April 1988.

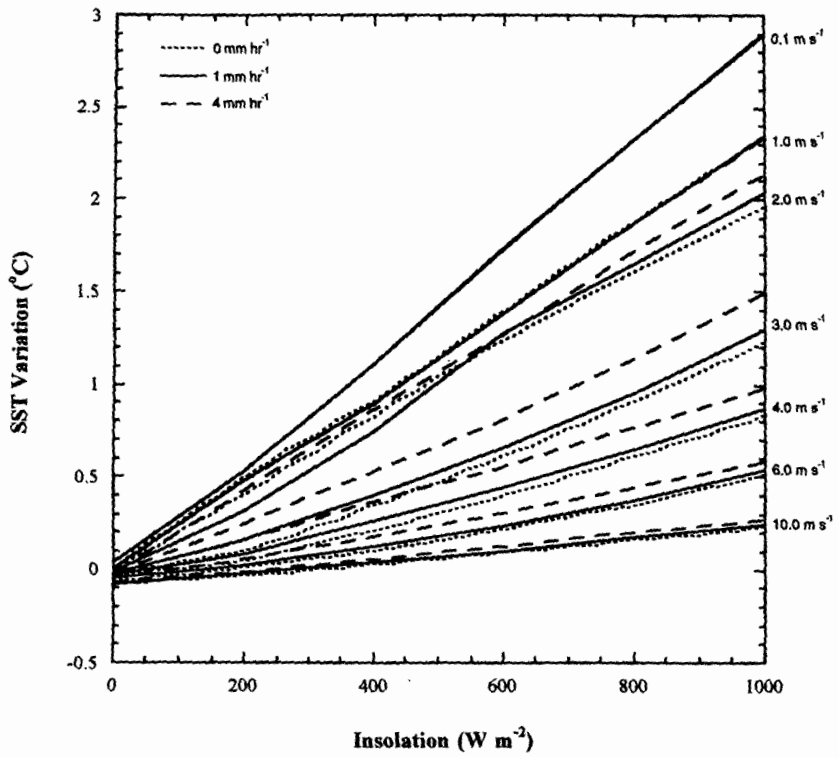

FIG. 11. The amplitude of the diurnal variation of the SST as a function of peak insolation for different values of wind speed and rainfall.

The warm pool (indicated by the 29°C isotherm) is seen to extend from the equatorial Indian Ocean eastward to a longitude of about 130°W. Values of the daily average surface wind speed (determined from the ECMWF analyses) and the peak solar insolation (determined from the Surface Radiation Budget dataset; Whitlock et al. 1993) are shown in Figs. 12a,b. Using (6), values of dSST are determined from the wind and solar insolation data and are shown in Fig. 12d. The effects of precipitation are ignored here. The impact of the magnitude of the surface wind are easy to see. In the north-central Pacific Ocean dSST $\sim$ 0, where the winds are strong. In regions of weak wind but strong insolation, amplitudes of dSST $>$ 1.5°C are seen. In fact, over most of the warm pool (SST $>$ 29°C), dSST $\geq$ 1°C.

6. Conclusions

A series of simulations using a one-dimensional ocean mixed layer model has been made to interpret the diurnal cycle of surface temperature in the tropical western Pacific. A blend of observations and the model is used to interpret the differences between the skin SST, the true bulk (1 cm) SST, the buoy (0.5 m) SST, and the ship (5.0 m) SST for different surface forcing. The following characteristics of the sea "surface" temperature were found:

- the difference between the skin and true bulk SST shows little variation over the diurnal cycle, with the skin SST being on average about 0.2°C cooler than the true bulk SST, although under conditions of high insolation and very low wind speed the skin SST may become slightly warmer than the true bulk SST;
- the difference between the skin and 0.5-m SST shows greater variation over the diurnal cycle, as the skin SST can become warmer during middle to high insolation periods and light winds
- the amplitude of the diurnal cycle is largest for the skin and true bulk SST relative to the buoy and ship SST, although the difference in amplitude is diminished for all temperatures is diminished for high surface wind speeds

TABLE 5. Coefficients for determination of diurnal sea surface temperature amplitude (dSST) from (6).

Coefficient	$U > 2$ m s^{-1} value	$U \leq 2$ m s^{-1} value
f	0.262	0.328
a	0.002 65	0.002
b	0.028	0.041
c	−0.838	0.212
d	−0.001 05	−0.000 185
e	0.158	−0.329

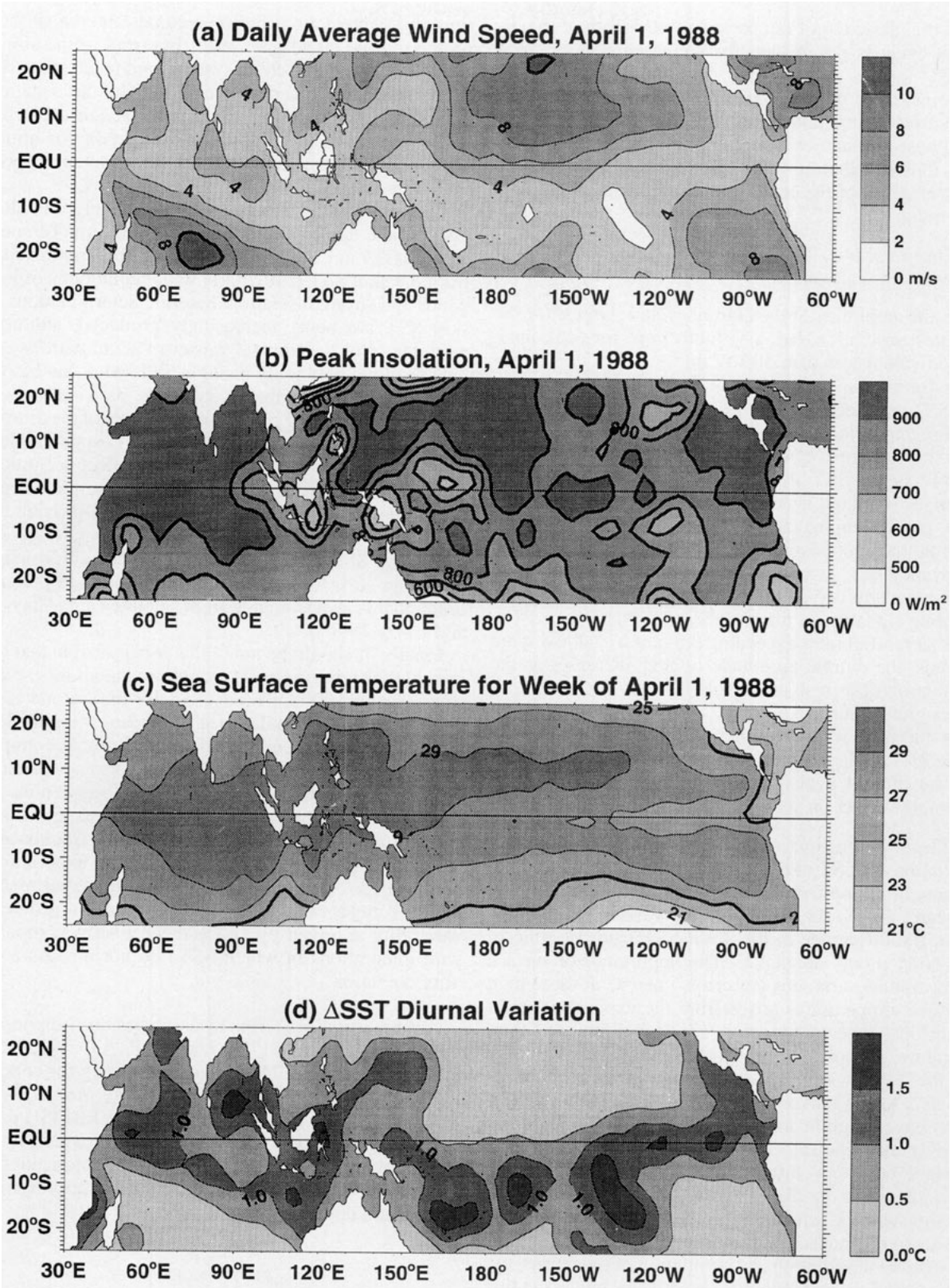

FIG. 12. Spatial distribution for 1 April 1988 for (a) daily averaged surface wind speed (from ECMWF), (b) peak surface insolation (from Surface Radiation Budget analysis), (c) sea surface temperature from the NOAA operational analysis, and (d) the parameterized amplitude of the diurnal SST variation obtained from (6).

- the phase lag of temperature with depth of the diurnal cycle is diminished for increased surface wind speed
- increased wind speed has a cooling effect on the sea surface temperature, both by decreasing the net surface heat flux and by increasing the upper-ocean mixing, thus distributing the surface heating throughout a greater depth of the ocean and diminishing the surface warming.

The amplitude of the diurnal cycle of SST was shown to be influenced in the following ways:

- the amplitude of the diurnal cycle is largest for the greatest insolation, being virtually zero for peak insolation values less than 300 W m^{-2}
- for wind speeds ≥ 10 m s^{-1}, the diurnal amplitude of SST is effectively zero, independent of insolation and precipitation values
- the influence of surface wind speed on the diurnal amplitude of SST is nonlinear and is influenced by changes in mixed layer depth
- the freshening and cooling associated with precipitation have opposing effects on the ocean surface buoyancy flux
- even short-lived precipitation events leave a local cooling signature at the surface
- at rainfall rates exceeding 0.5 mm h^{-1} at low wind speeds, the diurnal amplitude of SST increases as the formation of a fresh and stable layer at the surface allows greater surface heating
- the impact of precipitation on the diurnal amplitude of SST depends on when the precipitation occurs in the diurnal cycle, with nighttime rain having the strongest effect on surface cooling.

The following question arises from these results. Are variations of SST of the order of 1°–2°C on the diurnal timescale important in the tropical western Pacific Ocean? To put these temperature variations into context, the difference in the TWP SST from El Niño to La Niña is only about 1°C. The importance of surface temperature variations (or errors) of 1°C at these high surface temperatures arises from the exponential relationship between saturation vapor pressure and temperature. As pointed out in Table 1, a 1°C error in SST in the TWP will result on average in an error of 27 W m^{-2} to the surface energy balance. Such an error may have a significant impact on modeled atmospheric convection. The effect of such an error on the ocean surface buoyancy flux is further enhanced by the associated error to the evaporation component to the freshwater flux, which acts in the same direction as the errors to the surface heat balance.

Correct observation and simulation of the diurnal cycle of SST is undoubtedly essential to understanding and modeling the correct feedback between clouds and the SST. Because of the nonlinear relationships between clouds and the surface fluxes, incorrect simulation of the interactions between clouds and the surface on the diurnal cycle may result in errors to the simulation of larger-scale cloud systems and feedback to the large-scale atmospheric dynamics. The information provided here can be used to parameterize a diurnal SST cycle as a lower boundary condition for atmospheric models where sea surface temperature is specified climatologically or using observations.

Current SST climatologies are effectively climatologies of the upper ocean at a depth of 0.5 m. Temperatures at 0.5 m have been shown to differ significantly from the skin SST particularly under conditions of low winds and strong insolation. Satellite determinations of skin SST are being increasingly produced, although particularly in the tropical western Pacific with its extensive cloudiness, only a single SST value can be obtained for a period that is typically as long as two weeks. The sampling of different portions of the diurnal cycle in different regions can give rise to apparent horizontal variations in SST that do not reflect accurately the true horizontal variability. The data on the diurnal amplitude of skin SST presented here can provide the foundation for adding a diurnal cycle to satellite-derived skin SST values by using ancillary information regarding surface insolation, wind speed, and precipitation that is also available from satellite (e.g., Clayson and Curry 1996).

Finally, it should be noted that it is probable that the impact of the diurnal cycle rectifies to longer timescales (e.g., Zhang 1996). This is because the diurnal temperature increase results in a systematic bias in SST relative to the currently used SST values, the amplitudes of the SST variations are large scale and basically spatially coherent, and feedbacks occur between the atmosphere and ocean on the diurnal time scale. To test if the diurnal variations do rectify to low frequencies, we plan to conduct a series of numerical experiments with NOAA/NMC and ECMWF. In these experiments, the SST fields will be adjusted to possess a diurnal variability as given by (6) and the results compared with integrations in which SSTs do not possess a diurnal variation.

Acknowledgments. This research has been supported by DE-FG03-94ER61771 and NSF ATM-9223150. We are grateful to C. Fairall and M. Gregg for collecting and providing the data from the R/V *Moana Wave* and to F. Bradley for providing the SILVERFISH data. We also greatly appreciate assistance provided by P. Schlüssel on incorporating the skin parameterization in the ocean model. Comments on the manuscript from L. Kantha are appreciated.

REFERENCES

Andre, J. C., and P. Lacarrere, 1985: Mean and turbulent structures of the oceanic surface layer as determined from one-dimensional third-order simulations. *J. Phys. Oceanogr.*, **15,** 121–132.

Arking, A., and D. Ziskin, 1994: Relationship between clouds and sea surface temperatures in the western tropical Pacific. *J. Climate,* **7,** 988–1000.

Caldwell, D. R., and W. P. Elliot, 1971: Surface stresses produced by rainfall. *J. Geophys. Oceanogr.,* **2,** 145–148.

Cechet, C., 1993: Diurnal SST cycle in the western equatorial Pacific: Measurements made aboard the R/V *Franklin* during the TOGA-COARE and pre-COARE cruises. *AMOS Bull.,* **6,** 26–32.

Chu, P. C., and R. W. Garwood, 1991: On the two-phase thermodynamics of the coupled cloud–ocean mixed layer. *J. Geophys. Res.,* **96,** 3425–3436.

Clayson, C. A., and J. A. Curry, 1996: Determination of surface turbulent fluxes for TOGA COARE: Comparison of in situ measurement and satellite retrievals. *J. Geophys. Res.,* **101,** in press.

——, ——, and C. W. Fairall, 1996: Evaluation of turbulent fluxes at the ocean surface using surface renewal theory. *J. Geophys. Res.,* **101,** in press.

Coppin, P. A., E. F. Bradley, I. J. Barton, and J. S. Godfrey, 1991: Simultaneous observations of sea surface temperature in the western Pacific Ocean by bulk, radiative and satellite methods. *J. Geophys. Res.,* **96,** 3401–3409.

Fairall, C. W., J. B. Edson, S. E. Larsen, and P. G. Mestayer, 1990: Inertial-dissipation air–sea flux measurements: A prototype system using real time spectral computations. *J. Atmos. Oceanic Technol.,* **7,** 425–453.

——, E. F. Bradley, J. S. Godfrey, G. A. Wick, J. B. Edson, and G. S. Young, 1996a: Cool-skin and warm-layer effects on sea surface temperature. *J. Geophys. Res.,* **101,** 1295–1308.

——, ——, D. P. Rogers, J. B. Edson, and G. S. Young, 1996b: Bulk parameterization of air–sea fluxes for TOGA COARE. *J. Geophys. Res.,* **101,** 3747–3764.

Fu, R., A. D. DelGenio, W. B. Rossow, and W. T. Liu, 1992: Are cirrus clouds a "thermostat" for tropical sea surface temperatures? *Nature,* **358,** 394.

Galperin, B., L. H. Kantha, S. Hassid, and A. Rosati, 1988: A quasi-equilibrium turbulent energy model for geophysical flows. *J. Atmos. Sci.,* **45,** 55–62.

Garwood, R. W., 1977: An oceanic mixed layer model capable of simulating cyclic states. *J. Phys. Oceanogr.,* **7,** 455–468.

Gaspar, P., 1988: Modeling the seasonal cycle of the upper ocean. *J. Phys. Oceanogr.,* **18,** 161–180.

Gosnell, R., C. W. Fairall, and P. J. Webster, 1995: The sensible heat of rainfall in the tropical ocean. *J. Geophys. Res.,* **100,** 18 437.

Hartmann, D. L., and M. L. Michelson, 1993: Large-scale effects on the regulation of tropical sea surface temperature. *J. Climate,* **6,** 2049–2062.

Hu, Q., and D. A. Randall, 1994: Low-frequency oscillations in radiative–convective systems. *J. Atmos. Sci.,* **51,** 1089–1099.

Kantha, L. H., and C. A. Clayson, 1994: An improved mixed layer model for geophysical applications. *J. Geophys. Res.,* **99,** 25 235–25 266.

Kraus, E., and S. Turner, 1967: A one-dimensional model of the seasonal thermocline: The general theory and its consequences. *Tellus,* **19,** 98–106.

Large, W. G., J. C. McWilliams, and S. Doney, 1994: Oceanic vertical mixing: A review and a model with a nonlocal boundary layer parameterization. *Rev. Geophys.,* **32,** 363.

Lau, K.-M., and P. H. Chan, 1988: Intraseasonal and interannual variations of tropical convection: A possible link between the 40-day mode and ENSO. *J. Atmos. Sci.,* **45,** 950–972.

——, C.-H. Sui, M.-D. Chou, and W.-K. Tao, 1994: An inquiry into the cirrus-cloud thermostat effect for tropical sea surface temperature. *Geophys. Res. Lett.,* **21,** 1157–1160.

Leary, C. A., and R. A. Houze, 1980: The contribution of mesoscale motions to the mass and heat fluxes of an intense tropical convective system. *J. Atmos. Sci.,* **37,** 784–796.

Ledvina, D. V., G. S. Young, R. A. Miller, and C. W. Fairall, 1993: The effect of averaging on bulk estimates of heat and momentum fluxes for the tropical western Pacific Ocean. *J. Geophys. Res.,* **98,** 20 211–20 217.

Leetmaa, A., and M. Ji, 1989: Operational hindcasting of the tropical Pacific. *Dyn. Atmos. Oceans,* **13,** 465–490.

Lewis, M. R., M. E. Carr, G. C. Feldman, W. Esaias, and C. McClain, 1990: Influence of penetrating solar radiation on the heat budget of the equatorial Pacific Ocean. *Nature,* **347,** 543–545.

Lindstrom, E. J., R. Lukas, R. Fine, E. Firing, S. Godfrey, G. Meyers, and M. Tsuchiya, 1987: The western equatorial Pacific Ocean circulation study. *Nature,* **330,** 533–537.

Liu, G., J. A. Curry, and R. S. Sheu, 1995: Classification of clouds over the western equatorial Pacific Ocean using combined infrared and microwave satellite data. *J. Geophys. Res.,* **100,** 13 811.

Liu, W. T., K. B. Katsaros, and J. A. Businger, 1979: Bulk parameterization of air–sea exchanges of heat and water vapor including the molecular constraints at the interface. *J. Atmos. Sci.,* **36,** 1722–1735.

——, A. Zhang, and J. K. B. Bishop, 1994: Evaporation and solar irradiance as regulators of sea surface temperature in annual and interannual changes. *J. Geophys. Res.,* **99,** 12 623–12 637.

Lukas, R., 1991: The diurnal cycle of sea surface temperatures in the western equatorial Pacific. TOGA Notes, **2,** 1–5.

——, and E. Lindstrom, 1991: The mixed layer of the western equatorial Pacific ocean. *J. Geophys. Res.,* **96,** 3343–3357.

——, P. J. Webster, and M. Ji, 1995: The large-scale context for the TOGA Coupled Ocean–Atmosphere Response Experiment. *Meteor. Atmos. Phys.,* **56,** 3.

Machado, L. A. T., and W. B. Rossow, 1993: Structure, characteristics, and radiative properties of tropical cloud clusters. *Mon. Wea. Rev.,* **121,** 3234.

——, N. DesBois, and J.-Ph. Duval, 1992: Structure and characteristics of deep convective systems over tropical Africa and the Atlantic Ocean. *Mon. Wea. Rev.,* **120,** 392–406.

Mapes, B. E., and R. A. Houze, Jr., 1995: Diabatic divergence profiles in western Pacific mesoscale convective system. *J. Atmos. Sci.,* **52,** 1807.

McCreary, J. P., and P. Lu, 1994: Interactions between the subtropical and equatorial circulations. The subtropical cell. *J. Geophys. Res.,* **24,** 466–497.

McPhaden, M. J., and S. P. Hayes, 1991: On the variability of winds, sea surface temperature and surface layer heat content in the western equatorial Pacific. *J. Geophys. Res.,* **96,** 3331–3342.

Mellor, G. L., and T. Yamada, 1974: Hierarchy of turbulence closure models for planetary boundary-layers. *J. Atmos. Sci.,* **31,** 1791–1806.

——, and ——, 1982: Development of a turbulence closure model for geophysical fluid problems. *Rev. Geophys. Space Phys.,* **20,** 851–875.

Morel, A., and D. Antoine, 1994: Heating rate within the upper ocean in relation to its bio-optical state. *J. Phys. Oceanogr.,* **24,** 1652–1665.

Price, J. F., R. A. Weller, and R. Pinkel, 1986: Diurnal cycling: Observations and models of the upper ocean response to diurnal heating, cooling and wind mixing. *J. Geophys. Res.,* **91,** 8411–8427.

Ramanathan, V., and W. Collins, 1991: Thermodynamic regulation of ocean warming by cirrus clouds deduced from observations of the 1987 El Niño. *Nature,* **351,** 27–32.

Reynolds, R. W., and D. C. Marsico, 1993: An improved real-time global SST analysis. *J. Climate,* **6,** 114–119.

Schlüssel, P., H.-Y. Shin, W. J. Emery, and H. Grassl, 1987: Comparison of satellite-derived sea surface temperatures with in situ measurements. *J. Geophys. Res.,* **92,** 2859–2874.

——, W. J. Emery, H. Grassl, and T. Mammen, 1990: On the bulk-skin temperature difference and its impact on satellite remote sensing of sea surface temperature. *J. Geophys. Res.,* **95,** 13 341–13 356.

Soloviev, A. V., and P. Schlüssel, 1994: Parameterization of the cool skin of the ocean and of the air–ocean gas transfer on the basis of modeling surface renewal. *J. Phys. Oceanogr.,* **24,** 1339–1346.

——, and ——, 1996: Evolution of cool skin and direct air–sea gas transfer coefficient during daytime. *Boundary-Layer Meteor.*, **77,** 45–68.

Stephens, G. L., and P. J. Webster, 1979: Sensitivity of radiative forcing to variable cloud and moisture. *J. Atmos. Sci.*, **36,** 1542–1556.

Stephens, G., and A. Slingo, 1992: An air-conditioned greenhouse. *Nature,* **358,** 369–370.

Sun, D.-Z., and Z. Liu, 1996: Dynamic ocean–atmosphere coupling: A thermostat for the tropics. *Science,* in press.

TOGA COARE IPO 1992: TOGA COARE Operations Plan. UCAR, Boulder, CO.

Wallace, J. M., 1992: Effect of deep convection on the regulation of tropical sea surface temperature. *Nature,* **357,** 230–231.

Webster, P. J., 1994: The role of hydrological processes in ocean–atmosphere interactions. *Rev. Geophys.*, **32,** 427–476.

——, and R. Lukas, 1992: TOGA COARE—The coupled ocean and atmosphere response experiment. *Bull. Amer. Meteor. Soc.,* **73,** 1377–1416.

——, J. Loschnigg, and J. McCreary, 1996: Sea surface temperature regulation in the northern Indian Ocean: Counterpoint to the western Pacific Ocean. *Science,*

Whitlock, C. H., T. P. Charlock, W. F. Staylor, R. J. Pinker, J. Laszlo, R. C. DiPasquale, and N. A. Ritchey, 1993: WCRP Surface Radiation Budget Shortwave Data Product Description Version 1.1. NASA Tech. Memo. 107747.

Wick, G. A., W. J. Emery, and P. Schlüssel, 1992: A comprehensive comparison between satellite-measured skin and multichannel sea surface temperature. *J. Geophys. Res.*, **97,** 5569–5595.

Wick, G., 1995: Evaluation of the variability and predictability of the bulk minus skin SST difference with application to satellite-measured SST. Ph.D. thesis, University of Colorado, Boulder, 139 pp.

Williams, S., 1993: Central Equatorial Pacific Experiment (CEPEX), Operations Summary; 1993. UCAR/Office of Field Project Support.

Woods, J. D., W. Barkmann, and A. Horch, 1984: Solar heating of the oceans—diurnal, seasonal and meridional variation. *Quart. J. Roy. Meteor. Soc.,* **110,** 633–656.

Young, G. S., D. V. Ledvina, and C. W. Fairall, 1992: Influence of precipitating convection on the surface budget observed during a Tropical Ocean Global Atmosphere pilot cruise in the tropical western Pacific Ocean. *J. Geophys. Res.*, **97,** 9595–9603.

Zhang, C., 1993: Large-scale variability of atmospheric deep convection in relation to sea surface temperature in the Tropics. *J. Climate,* **6,** 1898–1912.

——, 1996: Coherence between SST and atmospheric variability in the western Pacific warm pool. Preprints, *Eighth Conf. on Air–Sea Interaction and Conf. on the Global Ocean–Atmosphere–Land System* (*GOALS*), Atlanta, GA, Amer. Meteor. Soc., J112–J116.